Photoacoustic Analysis of Proteins: Volumetric Signals and Fluorescence Quantum Yields

Elizabeth Kurian, Franklyn G. Prendergast, and Jeanne Rudzki Small
Department of Biochemistry and Molecular Biology, Mayo Foundation, Rochester, Minnesota 55905, and Department of Chemistry and Biochemistry, Eastern Washington University, Cheney, Washington 99004 USA

ABSTRACT A series of proteins has been examined using time-resolved, pulsed-laser volumetric photoacoustic spectroscopy. Photoacoustic waveforms were collected to measure heat release for calculation of fluorescence quantum yields, and to explore the possibility of photoinduced nonthermal volume changes occurring in these protein samples. The proteins studied were the green fluorescent protein (GFP); intestinal fatty acid binding protein (IFABP), and adipocyte lipid-binding protein (ALBP), each labeled noncovalently with 1-anilinonaphthalene-8-sulfonate (1,8-ANS) and covalently with 6-acryloyl-2-(dimethylamino)naphthalene (acrylodan); and acrylodan-labeled IFABP and ALBP with added oleic acid. Of this group of proteins, only the ALBP labeled with 1,8-ANS showed significant nonthermal volume changes at the $\beta = 0$ temperature (~3.8°C) for the buffer used (10 mM Tris-HCl, pH 7.5) (β is the thermal cubic volumetric expansion coefficient). For all of the proteins except for acrylodan-labeled IFABP, the fluorescence quantum yields calculated assuming simple energy conservation were anomalously high, i.e., the apparent heat signals were lower than those predicted from independent fluorescence measurements. The consistent anomalies suggest that the low photoacoustic signals may be characteristic of fluorophores buried in proteins, and that photoacoustic signals derive in part from the microenvironment of the absorbing chromophore.

INTRODUCTION

The ever-increasing use of fluorescent probes as tools in biology and chemistry has prompted us to examine the measurement of fluorescence quantum yields. Our goal has been to examine the use of time-resolved, pulsed-laser, volumetric photoacoustics in determining the fluorescence quantum yields of proteins. The method has been successful in the past for measuring quantum yields of dyes free in solution (Grabowski et al., 1992; Rothberg et al., 1983; Small et al., 1989; Small and Larson, 1990), but not always for dyes bound to proteins (Small and Larson, 1990). There are several possible reasons known for photoacoustic signals being anomalously large or small. Usually these seemingly anomalous results are due to nonthermal volume changes that may be isolated from thermally induced changes at the "$\beta = 0$" temperature of water, around 4°C. At this temperature, heat release contributes negligibly to photoacoustic waveforms, and any observed signal is due to a nonthermal volume change, such as a molecular conformational change with or without associated solvent reorganization (Small and Kurian, 1995).

The overarching goal of this study was to evaluate the applicability of the photoacoustic technique to the measurement of protein fluorescence quantum yields. The photoacoustic method used for this purpose does not rely on the measurement of light emerging from the photoexcited sample, in contrast to common fluorescence methods. Instead, processes concomitant with fluorescence are measured. The heat released by the photoexcited samples results in solvent expansion, creating an ultrasonic pressure wave (or multiple waves). The photoacoustic experiment uses a transducer to measure the ultrasound, both in frequency and magnitude, thereby to quantify the heat originally released to solution. As for steady-state measurement of fluorescence quantum yields, the photoacoustic experiment uses a standard for comparative purposes. The reference standard is optimally a nonfluorescent compound that absorbs light and quickly releases all absorbed energy as heat to solution during decay of the excited state. For equally absorbing reference and fluorescent sample solutions, the fluorescent sample generally shows smaller photoacoustic waveforms, with the "missing" energy being attributed to the fluoresced light, which by definition does not contribute to the photoacoustic signal. Conservation of energy is then invoked to calculate the fluorescence quantum yield, Φ_{fl}: knowing the ratio of the amplitude of the sample waveform to that of the reference waveform, and knowing the median fluorescence emission wavelength (the emission maximum wavelength is usually an adequate estimate for this), one can simply calculate Φ_{fl} (Small et al., 1989). For simple fluorescent dyes, with negligible intersystem crossing and hence little triplet formation and decay, the photoacoustic method works very well for quantitation of fluorescence quantum yields. In other words, recovered Φ_{fl} values agree very well with those obtained by the fluorescence comparison method (Small et al., 1989; Small and Larson, 1990). In principle, for room temperature measurements, all of the requisite data can be collected and analyzed in ~30 min. In comparison to methods using quinine sulfate, very stable reference compounds are used for photoacoustic measurements, thus ob-

Received for publication 18 September 1996 and in final form 23 January 1997.

Address reprint requests to Dr. Jeanne Rudzki Small, Department of Chemistry and Biochemistry, Mail Stop 74, Eastern Washington University, 526 5th St., Cheney, WA 99004-2431. Tel.: 509-359-2257; Fax: 509-359-6973; E-mail: jsmall@ewu.edu.

0006-3495/97/07/466/11 $2.00

viating the need for extensive solution preparation each time a Φ_{fl} measurement is made.

However, for estimations of fluorescence quantum yields, photoacoustic signals originating from heat may be complicated by superimposed signals from solvation changes and/or molecular conformational changes (Small and Kurian, 1995). In principle, any process that creates a rapid volume change (expansion or contraction) can generate a photoacoustic signal. Thus a photoacoustic waveform observed at room temperature may have originated from solvent expansion due to heat release only, or to concurrent volumetric processes. The direction in which and degree to which a solvent expands or contracts upon absorbing heat are characterized by the parameter β, the thermal cubic volumetric expansion coefficient. Nonaqueous solutions expand when heated (i.e., they are characterized by having $\beta > 0$). Aqueous solutions also expand when heated, provided the initial temperature is above 4°C. Below 4°C, water contracts when heated ($\beta < 0$). For aqueous solutions, it is possible to work at the $\beta = 0$ temperature (around 4°C) to look for nonthermal signals. Any signal observed at this temperature must be due to processes other than heat release, processes that may be extremely interesting in their own right. With the knowledge of the presence or absence of nonthermal contributors obtained from $\beta = 0$ measurements, it is possible to more accurately interpret the data at higher temperatures, where Φ_{fl} measurements are usually made.

Our strategy for this study was to measure the apparent Φ_{fl} at a variety of temperatures (7°C, 15°C, 25°C, 35°C) using both the standard fluorescence method as well as the photoacoustic technique, for the several fluorescent proteins selected. The proteins were also studied photoacoustically at the $\beta = 0$ temperature and other selected temperatures to assess the extent of nonthermal contributors to photoacoustic heat signals. With these data, the Φ_{fl} values from the two methods were examined for internal consistency. In the case of consistent disparities, we assumed that the Φ_{fl} from the fluorescence measurements were fundamentally correct, and that anomalous photoacoustic data must be due to alterations of the acoustic generation induced by some facet of the protein solution.

We have embarked on a detailed analysis of the photoacoustic signals from a variety of dyes and proteins, at the $\beta = 0$ temperature and at higher temperatures, to determine the extent to which nonthermal volume changes influence fluorescence quantum yield calculations made from photoacoustic data.

Included in this study are the green fluorescent protein (GFP), which contains an unusual intrinsic fluorophore; intestinal fatty acid-binding protein (IFABP), and adipocyte lipid-binding protein (ALBP), each labeled noncovalently with 1-anilinonaphthalene-8-sulfonate (1,8-ANS) and labeled covalently with 6-acryloyl-2-(dimethylamino)naphthalene (acrylodan) and acrylodan-labeled IFABP and ALBP with added oleic acid.

GFP is the green light emitter in the bioluminescence of the jellyfish *Aequorea victoria* (Ward, 1979). The protein has absorbance maxima at 395 nm (the principal absorbing band) and a smaller peak at 475 nm. The fluorescence emission maximum occurs at 509 nm, with a shoulder at 545 nm (Ward et al., 1980). The intense fluorescence (quantum yield > 0.9) of this protein is attributed to a covalently bound chromophore, which is a postribosomal modification of the amino acid sequence of the protein. The protein also contains one tryptophan residue (Prasher et al., 1992), which is generally undetected in fluorescence measurements, probably because of energy transfer (essentially 100% efficient) of the tryptophan fluorescence to the green fluorescent chromophore. The postribosomal modification in the primary structure of the protein occurs at residues 66–68 and involves covalent modification of a Ser-Gly-Tyr tripeptide, which is cyclized with the loss of a water molecule to form an extended imidazolopyrazinone ring structure that comprises the chromophore. GFP coexists in vivo with the calcium-triggered photoprotein aequorin, which is the energy donor for the green fluorescence normally emitted by the organism.

IFABP and ALBP belong to a class of intracellular lipid binding proteins (for a review see Banaszak et al., 1994). Several of these proteins have been isolated from a variety of tissues and organisms; they bind free fatty acids and other lipids with high affinity. Members of the family vary in their specificities for the various ligands. The physiological functions of the fatty acid-binding proteins remain unclear, although a protective role against the deleterious effects of free fatty acids in the cell has been postulated (Ockner, 1990). The x-ray crystal structures of several of these proteins (both apo and holo forms) have been solved. The 3D structures of the proteins in this family are all remarkably similar, even though primary sequence homology ranges from 20% to 80%. They are folded into a single domain with a β-barrel motif, and the ligand is contained within a cavity formed by the β-barrel. The cavity does not mirror the shape of the ligand and is larger than the volume needed to accommodate the ligand. More than 20 water molecules identified by x-ray crystallography are present in the binding cavity in the absence of the fatty acid ligand, although, depending on how the "pocket" is defined, there is potential space for as many as 50 water molecules. With fatty acid, the number of water molecules "seen" in the cavity crystallographically falls to about four, implying, at the very least, substantial solvent reorganization and probably substantial loss of water from the binding cavity. To study the proteins using fluorescence, we labeled them covalently with acrylodan and noncovalently with 1,8-ANS.

Acrylodan is a thiol-selective fluorescent compound that is used primarily to modify cysteine residues in proteins (Prendergast et al., 1983). The quantum yield of this compound is greatly enhanced upon reaction with thiols, and the fluorescent derivatives are highly sensitive to dipolar perturbation from their environments. Thus acrylodan is useful

in the study of hydrophobic domains, conformational changes, and dipolar relaxation processes in proteins.

1,8-ANS is also a polarity-sensitive fluorescent dye that has been used extensively in the characterization of hydrophobic binding sites in proteins. 1,8-ANS binds noncovalently to the ligand-binding sites of several proteins, often with high affinity, and generally the fluorescence of the 1,8-ANS–protein complex is enhanced severalfold compared to that of 1,8-ANS in aqueous medium. The fluorescence of 1,8-ANS is also markedly enhanced in nonpolar solvents such as ethanol, methanol, dioxane, and acetonitrile, and in water mixtures of these solvents (Slavik, 1982).

IFABP and ALBP were covalently labeled with acrylodan. Acrylodan binds ALBP at Cys^{117}, as determined by amino acid analysis of tryptic digests of labeled and unlabeled ALBP (E. Kurian, unpublished results). IFABP does not contain any cysteines, but under appropriate solvent conditions, acrylodan binds to IFABP Lys^{27} (Richieri et al., 1992). We have verified this specific binding of acrylodan to IFABP by mass spectrometry (Kurian et al., 1996) and amino acid analyses of tryptic digests of labeled and unlabeled IFABP (E. Kurian, unpublished results).

MATERIALS AND METHODS

Materials

Acrylodan was obtained from Molecular Probes (Eugene, OR). 1,8-ANS was obtained from Fluka (Ronkonkoma, NY). Oleic acid was from Avanti Polar Lipids (Birmingham, AL). Horse skeletal muscle metmyoglobin was obtained from Calbiochem (La Jolla, CA). Buffer salts and solvents were obtained from Sigma (St. Louis, MO). Quinine sulfate was from Eastman Chemicals (Rochester, NY). Phenyl Sepharose was obtained from Pharmacia (Piscataway, NJ). Some of the GFP we used was kindly provided by Dr. William W. Ward (Rutgers University, New Brunswick, NJ). The rest was further purified from a freezer stock left over from an extract in the purification of aequorin (Blinks et al., 1978). Fluorescein from Eastman Chemicals (Rochester, NY) was purified by thin-layer chromatography (fluorescein was dissolved in 0.1 N NaOH; the eluting mixture was *t*-butanol, *n*-butanol, and ammonium hydroxide in the ratio 4:3:3) and used as in Kirk (1986).

Protein expression and purification

GFP

Partially purified GFP was stored at −70°C in a 10 mM EDTA/sodium acetate/NaCl buffer. The protein solution was thawed, concentrated, and dialyzed into 20 mM TES (*N*-tris[hydroxymethyl]methyl-2-aminoethanesulfonic acid) buffer (pH = 7.0). The solution was then applied to a phenyl sepharose column (10 cm × 2 cm) equilibrated with 20 mM TES at pH 7.0. The protein was eluted with 1% acetonitrile and further dialyzed against 10 mM Tris at pH 7.5. Purity was determined by its migration as a single band on sodium dodecyl sulfate-polyacrylamide gel electrophoresis, and spectrophotometric absorbance at 395 nm and 280 nm, with a final ratio $A_{395}/A_{280} > 1$.

Fatty acid-binding proteins

IFABP was overexpressed and purified as in (Kirk et al., 1996). We obtained a clone of ALBP from Dr. David Bernlohr (University of Minnesota, St. Paul, MN). The vector containing the ALBP gene was retransfected into the *Escherichia coli* strain MG1655. ALBP was expressed and purified by the procedure used for IFABP expression and purification.

Acrylodan labeling

IFABP was covalently labeled with acrylodan using the method of Richieri et al. (1992). ALBP was covalently labeled with acrylodan according to the method given in Prendergast et al. (1983). Purified IFABP was dialyzed against 10 mM sodium borate, 150 mM KCl at pH 9.0, and purified ALBP was dialyzed against 10 mM HEPES, 50 mM KCl, 20 μM dithiothreitol (pH 7.5). A 20 mM stock solution of acrylodan in dimethyl formamide (DMF) was added slowly over a period of 20 min to ~2 mg/ml solutions of IFABP and ALBP at 4°C. The molar ratio of protein to acrylodan in the final solutions was 1:3. The reaction was allowed to proceed for 48 h in the dark at 4°C. Uncomplexed acrylodan was removed by extensive dialysis. The efficiency of labeling for IFABP, calculated from the ratio of protein absorbance at 280 nm (ε = 16,900 cm^{-1} M^{-1}) and acrylodan absorbance at 360 nm (ε = 10,600 cm^{-1} M^{-1}), was greater than 90%. For ALBP (ε = 15,500 cm^{-1} M^{-1} at 280 nm), the efficiency of labeling was almost 100%.

1,8-ANS labeling

IFABP and ALBP were complexed with 1,8-ANS by adding a fivefold molar excess of protein to a 1,8-ANS solution. This was done to ensure that all of the 1,8-ANS in the solution was bound to the protein. The solutions were then diluted to give an optical density of ~0.3 at 366 nm for the photoacoustic measurements, and 0.1 at 370 nm for the fluorescence measurements.

Fluorescence measurements and analysis

The fluorescence quantum yield measurements were made on a Perkin-Elmer MPF-66 steady-state fluorometer. Samples used for photoacoustic measurements were diluted to give an optical density of 0.1 at 370 nm. A solution of quinine bisulfate in 0.1 N H_2SO_4 was used as the fluorescence standard. The corrected, integrated emission spectra (375–650 nm) were used to calculate the fluorescence quantum yield of each of the samples according to the method of Demas and Crosby (1971). The measurements were made at 15°C, 20°C, 25°C, and 35°C.

Photoacoustic measurements and analysis

The experimental apparatus for pulsed-laser photoacoustic measurements is shown in Fig. 1. Photoexcitation is achieved by the output of a nitrogen-pumped dye laser (model PL2300/PL202, 500-ps pulse width; Photon Technology International) operated at a 2- to 3-Hz repetition rate. The dye laser is operated with BPBD (365 nm) laser dye in toluene, with actual output measured as 366.6 nm. For work with GFP, the laser dye C500 in *p*-dioxane (475 nm) was used, with actual output measured at 475.3 nm. The laser pulse is divided by a beam splitter, so that ~1–15 μJ is incident on the sample cuvette, depending on which neutral-density filter is selected (filter selection is 0, 0.25, 0.5, and 1.0 optical densities, for 100%, 56%, 32%, and 10% transmittances, respectively), whereas ~8 μJ is diverted to a pyroelectric energy meter probe (Laser Precision Corporation/Laser Probe, RjP-735), position R ("Reflected") (Fig. 1). The energy meter (Laser Precision Corporation/Laser Probe, Rj-7620) reading of the energy probe-R input thus provides a measure proportional to the pulse energy incident on the sample and is used to correct for slight pulse-to-pulse variations in pulse light energy. A second, silicon-detector energy meter probe (Laser Precision Corporation/Laser Probe, RjP-765) is positioned beyond the sample cuvette, position T ("Transmitted") in Fig. 1. Energy probe-T values are used in Beer's law calculations of in situ sample absorbance.

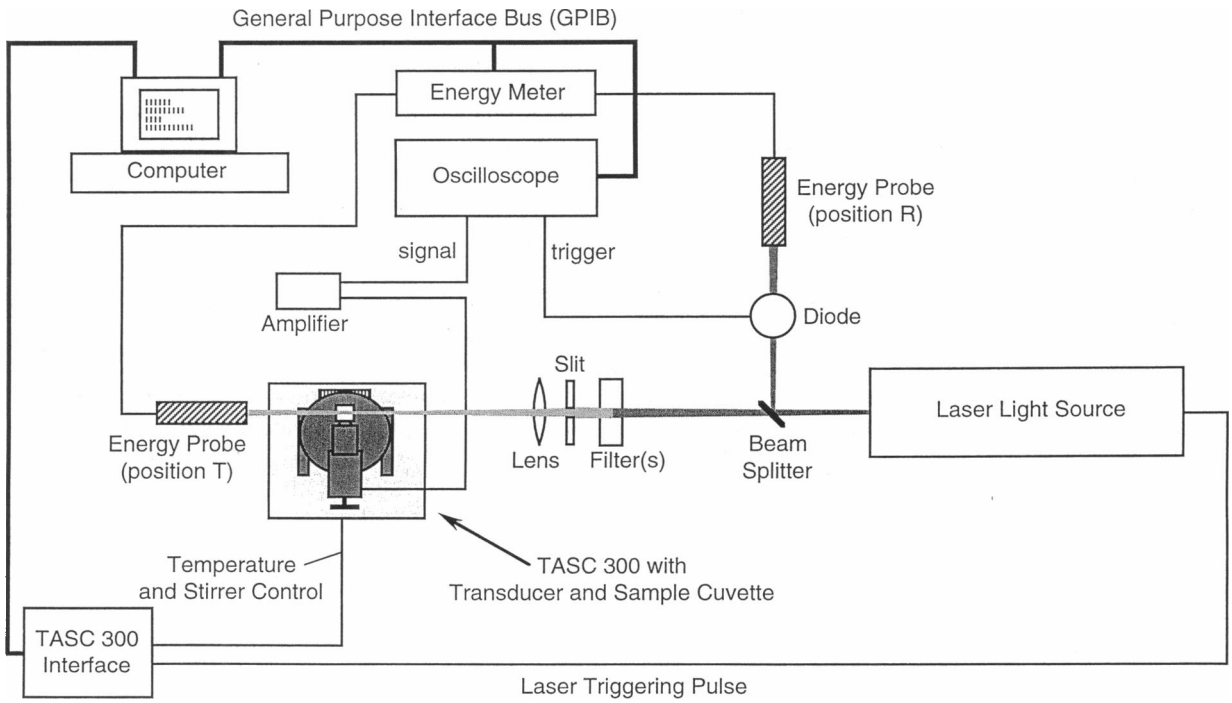

FIGURE 1 Schematic diagram of the pulsed-laser photoacoustic instrument.

The sample is contained in a standard, 1-cm path-length quartz absorbance cuvette equipped with a micro magnetic spin bar. A cylindrical lens (15-cm focal length) is positioned 13 cm before the front surface of the cuvette to give a thin, vertical slit of light (~11 mm by <0.5 mm) passing through the cuvette, parallel to the side walls of the cuvette. The cuvette is placed within a TASC 300 photoacoustics sample chamber (Quantum Northwest) equipped with a 1-MHz, broadband, heavily damped transducer (Panametrics, V-103). The acoustic interface between the cuvette sidewall and the transducer is provided by either silicone grease or ethylene glycol. Both acoustic couplants give comparable performance. For strongly fluorescent samples, a layer of aluminum foil is placed between the cuvette and the transducer, with acoustic couplant placed at all interfaces. Care is taken not to disturb the cuvette/transducer arrangement while changing samples. A very thin thermocouple probe (Yellow Springs Instruments model 555), attached to one input of a dual-probe digital thermometer (Cole-Parmer model 8402-20), is positioned inside the sample cuvette at all times to monitor sample temperature. The thin thermocouple probe was previously calibrated against a VWR Scientific model 1146 circulating water bath with digital temperature control, as well as the digital thermometer with a more standard thermocouple probe (Yellow Springs Instruments model 401) attached to the second input position. The uncertainty of the measured cuvette temperature is estimated as ±0.2°C.

In addition to positioning the sample cuvette relative to the laser pulses, the TASC 300 sample chamber provides temperature control and magnetic stirring by means of a computer interface. The TASC 300 internal metal temperature was checked using a Yellow Springs Instruments model 427 contact probe attached to the digital thermometer. Samples were kept air-saturated, and air flow was maintained in the TASC 300 at lower temperatures to reduce condensation.

Acoustic signals, generated by the light pulses and detected by the transducer, are amplified (Panametrics model 5662 ultrasonic preamplifier, 0.5–5 MHz, 54-dB gain) and digitized by a Tektronix model 2430 digital oscilloscope. The oscilloscope is triggered using a photodiode-based optical trigger (Laser Photonics L-OT) positioned between the beam splitter and energy probe-R (Fig. 1). The oscilloscope is operated at 10 ns per channel ("point"), 1024 channels per record, and 2–200 mV/division (8-bit vertical resolution). The mV/division setting is chosen for each sample to maximize the signal on the oscilloscope screen. Corrections are made for varying mV/division settings using the data collection software. Data from 100 to 500 laser pulses are averaged to give one photoacoustic waveform. The data are collected and processed with SOUND 3000 photoacoustics software (Quantum Northwest), capturing waveforms and energy readings over a National Instruments GPIB interface bus.

The optical densities of the reference and sample compounds are adjusted to be within 5% of each other to ensure that the photoacoustic waveform generation has the same geometrical configuration for both the reference and sample waveforms (Small et al., 1992). Solution optical densities between 0.1 and 0.8 at the photoexcitation wavelength of 366.6 nm (or 475.3 nm) are commonly used. Absorbance values are taken from measurements using either an independent laboratory spectrophotometer (Hitachi model U-2000) or in situ using values returned by the energy probes R and T (see Fig. 1) and the SOUND 3000 photoacoustics software (Quantum Northwest), which assumes the experiment to function as a single-beam spectrophotometer. The data required for a photoacoustics experiment include digitized waveforms for the reference and sample compounds; average energy meter readings measured concomitant with those waveforms; a waveform baseline collected for 100 laser pulses with no laser light incident on the cuvette; and either the reference and sample optical densities at the excitation wavelength measured independently, or the energy meter readings measured with solvent only in the cuvette, to calculate reference and sample solution absorbances in situ.

For each of the fluorescent protein samples, data (not shown) were collected using two neutral density filters of 100% and 56% transmittance (filter wheel positions 1 and 2), so that ~15 or 8 μJ, respectively, of light was incident on the sample cuvette. Analysis of data obtained at these two settings showed little difference in the calculated values for amplitudes and fluorescent lifetimes. This laser energy range has been found to generate few photochemical artifacts in photoacoustic data, even for photochemically sensitive samples such as carboxymyoglobin and benzophenone triplet (Rudzki, 1985). Sample optical densities measured before and after the photoacoustics experiments were found to be the same, indicating that no photobleaching had occurred during photoexcitation.

Data analysis is performed using the Sound Analysis 3000 nonlinear least-squares deconvolution analysis program (Quantum Northwest),

which utilizes the mathematical model presented by Small et al. (1992). The deconvolution analysis assumes that the transducer response function is given by the reference waveform, R, generated by photoexciting a sample that absorbs light and rapidly releases the absorbed energy as heat (within 1 ns). The sample waveform, S, may have several time constants, τ_i, and amplitudes, ϕ_i, for thermal and/or volumetric decays, which are assumed to sum as the function $h(t)$: $h(t) = \Sigma_i\ \phi_i\ (1/\tau_i)\ \exp\ (-t/\tau_i)$. The deconvolution program uses the relationship $S(t) = R(t)*h(t)$, where $*$ represents the convolution function, to analyze the reference and sample waveforms together to yield ϕ_i and τ_i parameters.

Raw oscilloscope data must be prepared for deconvolution analysis. After the baseline is subtracted from the raw waveforms, the reference and sample waveforms are corrected for small variations in sample absorbance and average laser pulse energy. The maximum of the reference waveform is scaled to unity for clarity, and the same scaling factor is applied to the sample waveform. Within the 1024 channels of data, a region is selected that represents the highest signal-to-noise ratio for the acoustic data, usually the complete vibrational response of the transducer in response to the first sound wave to reach it after laser firing. Deconvolution is performed for one to four components, with goodness of fit judged by the mean of the squared residuals (MSR), the appearance of the residuals, and the appearance of the autocorrelation function (Small et al., 1992). Slight shift (time axis) and baseline (vertical axis) corrections are incorporated when needed to improve the fitting. The time-axis shift corrections are useful for fitting nonrandom errors such as slight speed-of-sound differences between reference and sample waveforms. The vertical-axis (baseline) corrections move the reference waveform up or down slightly relative to the sample waveform to accommodate slight differences in waveform digitization of reference and sample waveforms.

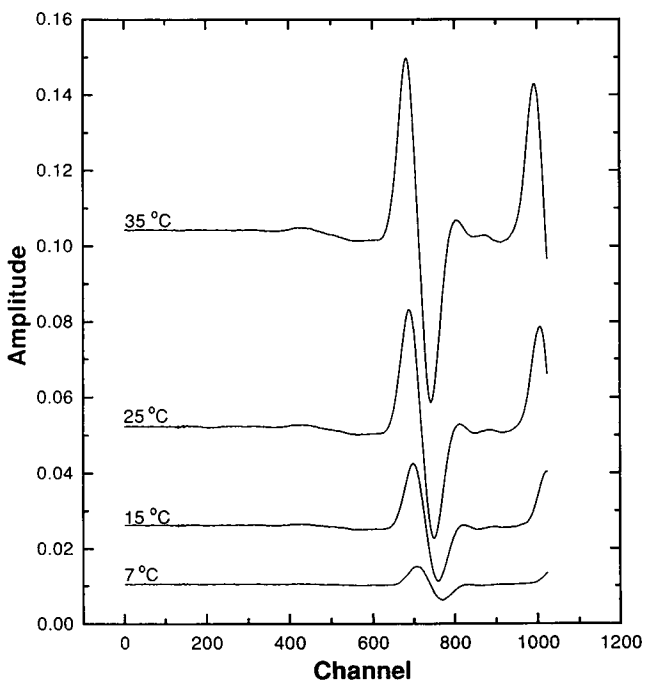

FIGURE 2 Photoacoustic waveforms of metmyoglobin in 10 mM Tris-HCl, pH 7.5, at a variety of temperatures, after photoexcitation with about 10 μJ of 366.6 nm light. Each channel represents 10 ns. A total of 1024 channels are digitized, with laser firing occurring at channel 128. The amplitude is in arbitrary units.

RESULTS

Temperature dependence

The strong temperature dependence of photoacoustic waveforms in aqueous solutions is illustrated in Fig. 2, where the reference compound metmyoglobin is used to quickly and efficiently convert absorbed light energy into heat (Small and Kurian, 1995). The acoustic waves represented in Fig. 2 are thus attributed to bulk solvent properties in response to heat release. Dominant among aqueous solvent thermoelastic properties in temperature dependence is the thermal cubic volumetric expansion coefficient, $\beta = \mathrm{d}\ \ln\ V/\mathrm{d}T$, where V is volume and T is temperature (Adelhelm et al., 1990). For example, pure water exhibits β values of -68, 0, 46, and 346 ($10^{-6} \cdot K^{-1}$) at 0, 3.9, 7, and 35°C, respectively (Weast, 1974), whereas its values for density and heat capacity remain essentially constant. The amplitude of the photoacoustic waveforms in Fig. 2 may be used to represent the β values for the particular solvent used, 10 mM Tris-HCl, pH 7.5, which has a $\beta = 0$ temperature of 3.8°C, and other values similar to those of pure water. Thus, although

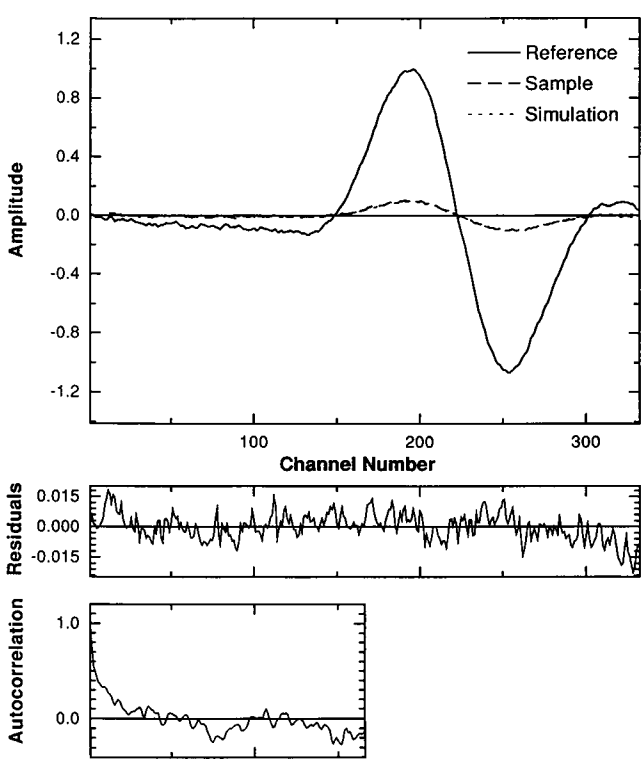

FIGURE 3 Deconvolution analysis of photoacoustic waveforms of metmyoglobin (reference) and GFP (sample) at 35°C in 10 mM Tris-HCl, pH 7.5. Each channel represents 10 ns. Photoexcitation was achieved using 15-μJ pulses of 475.3-nm light. Both reference and sample waveforms have been processed to account for differences in oscilloscope digitization parameters, sample absorbance, and laser pulse energies. The simulated waveform is superimposed on the GFP sample waveform and was calculated by convolution of the reference waveform with an exponential decay $\phi/\tau \cdot \exp(-t/\tau)$ (Small et al., 1992), incorporating the "best fit" parameters of $\phi = 0.097$ and $\tau < 20$ ns. The residuals and the autocorrelation of the residuals indicate a reasonable, one-component fit.

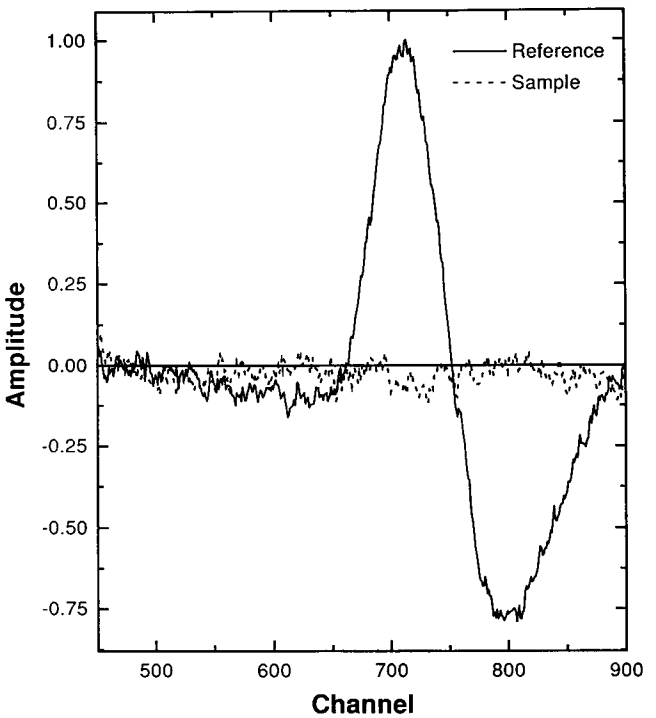

FIGURE 4 Example of a sample photoacoustic waveform at the $\beta = 0$ temperature of 3.8°C, indicating a lack of nonthermal volumetric effects. Each channel represents 10 ns. The sample compound is acrylodan-labeled IFABP at 3.8°C, and the reference compound is metmyoglobin at 7°C.

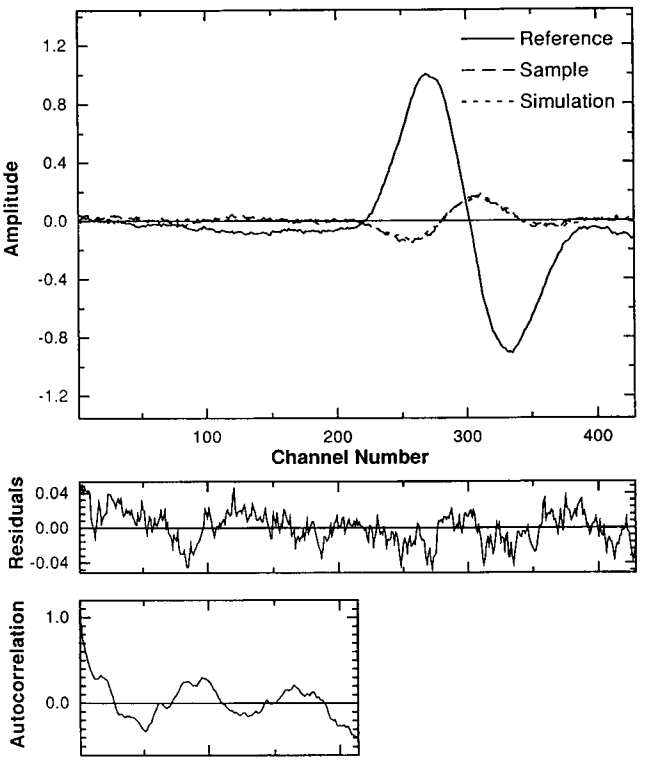

FIGURE 5 Photoacoustic waveforms of metmyoglobin (at 7°C) and 1,8-ANS-labeled ALBP (at 3.8°C). Each channel represents 10 ns. The panels are analogous to those in Fig. 3. To analyze the sample waveform, the metmyoglobin reference waveform was first shifted to the right by +4 channels to account for speed-of-sound differences in the solvent (10 mM Tris-HCl, pH 7.5) between 7 and 3.8°C. The effect of temperature on the speed of sound in aqueous solutions is apparent by the leftward shift of the waveforms with increasing temperature in Fig. 2. The shift of +4 channels was determined by careful measurement of metmyoglobin waveforms at 7°C and 3.8°C, and was used for all $\beta = 0$ analyses.

it is not shown in Fig. 2, the photoacoustic waveform of the metmyoglobin solution at 3.8°C is flat (null); below 3.8°C the signal is progressively negative with decreasing temperature.

In Fig. 2 the waveforms shift slightly to the left (i.e., to shorter times) as the temperature increases because of the faster speed of sound at higher temperatures. Speed-of-sound increases are also responsible for the start of the second oscillating waveform emerging at the right of Fig. 2 at higher temperatures: whereas the dominant oscillating waveform represents the ultrasound generated in the cuvette and passing directly toward the transducer, the second oscillating waveform represents the sound wave that emerged in the direction of the far sidewall of the cuvette, and which had to reflect from that sidewall before traveling in the direction of the transducer.

At a given temperature, differences between two photoacoustic waveforms may be analyzed by deconvolution to yield parameters relating to the extent of volume change (e.g., due to heat release) and to the rate of volume change. Fig. 3 shows this analysis for GFP. In light of data discussed below, we expect that the photoacoustic waveforms of both GFP and metmyoglobin to be uncomplicated by nonthermal contributions. Thus, because the processed GFP waveform has an amplitude only ~10% that of metmyoglobin, we conclude that the highly fluorescent GFP releases only a small fraction of its absorbed photon energy to solution as heat. As noted above, simple energy conservation considerations suggest that what is not released as heat must be released as light: the more fluorescent the sample, the smaller the photoacoustic waveform. This inference was consistent throughout our experiments, with the less fluorescent samples such as 1,8-ANS-labeled IFABP, acrylodan-labeled IFABP, and acrylodan-labeled IFABP with bound oleic acid having progressively larger photoacoustic waveforms, with magnitudes between those of metmyoglobin and GFP. Degassing the protein solutions with argon resulted in no perceptible change in the photoacoustic waveforms.

To interpret the photoacoustic data at higher temperatures (e.g., at 25°C) it was necessary to examine all of the protein solutions at the $\beta = 0$ temperature of 3.8°C. All proteins except one showed waveforms similar to that displayed in Fig. 4. The reference compound is metmyoglobin at 7°C, which itself gives a relatively small waveform (see Fig. 2). The metmyoglobin is maintained at 7°C rather than at 3.8°C (where the waveform would be zero) to have a distinguishable positive waveform to compare with potentially null sample waveforms. As seen in Fig. 4, at 3.8°C, the acrylodan-labeled IFABP waveform is essentially flat within the experimental noise and thus is considered to be nonexistent.

The notable exception to the $\beta = 0$ null protein waveforms is 1,8-ANS-labeled ALBP (Fig. 5). Not only is there a nonzero sample waveform at 3.8°C, the observed waveform is two-component in nature, with an initial, large contraction (recovered as $\tau_1 \leq 1$ ns, but best described as simply being less than our time resolution of ~20 ns), followed by an equal-but-opposite expansion ($\tau_2 \approx 35$ ns). The photoacoustic data for 1,8-ANS-labeled ALBP at higher temperatures, where heat is expected to contribute to the photoacoustic waveforms, were difficult to analyze unless the volumetric behavior at 3.8°C was taken into account. Examination of the entire temperature range of data leads to the conclusion that the fast component appears to represent a volumetric contraction at $\beta = 0$, and heat release plus volume contraction at higher temperatures, whereas the slower component appears to represent a volumetric expansion at all temperatures.

Importantly, no photoacoustic waveform was observed for 1,8-ANS dissolved in buffer at 3.8°C, nor was any observed for 1,8-ANS bound to IFABP. This does not mean that the contraction/expansion phenomenon does not occur in these other systems; it may be that the contraction/expansion is too rapid to be resolved with our time resolution limit of <20 ns. Because most of the fluorescence quantum yield measurements relied on the use of quinine sulfate as a standard, a solution of quinine sulfate in 0.1 N H_2SO_4 at its $\beta = 0$ temperature of 2.7°C was also examined photoacoustically. Again, no waveform was observed, thus indicating no unusual properties of this fluorophore. (In contrast, the fluorophore 8-hydroxypyrene-1,3,6-trisulfonic acid demonstrates a dramatic $\beta = 0$ waveform, consistent with its known photochemical behavior (Small and Kurian, 1995).)

In general, the decay times recovered for heat release from the photoexcited proteins were substantially less than our time resolution of ~20 ns. For rapid decays, the computer program usually reports recovered lifetimes, τ_i, of 5–10 ns, typical for fast heat release when the digitization channel width is 10 ns (Small et al., 1992). This was different for 1,8-ANS bound to IFABP, which consistently showed decay times on the order of 15–20 ns. Attempts at resolving this decay into two components were not successful. However, this fast decay of 15–20 ns is in agreement with the fluorescence lifetime of the IFABP-1,8ANS complex measured by time-resolved fluorescence (Kirk et al., 1996). Thus the photoacoustic data for the protein systems studied have generally shown fast decays of 5–10 ns when the actual fluorescence lifetime was less than 10 ns, and ~15–20 ns when the fluorescence lifetime was in that time region.

Table 1 summarizes the photoacoustic data in terms of fluorescence quantum yields and compares the fluorescence quantum yields measured by photoacoustics, $\Phi_{fl}(PA)$, with those measured by standard fluorescence methods, $\Phi_{fl}(fl)$. A simple equation is used to convert a sample's relative photoacoustic amplitude for fast heat release, ϕ, along with fluorescence and excitation wavelengths, λ_{fl} and λ_{ex}, into $\Phi_{fl}(PA)$: $\Phi_{fl}(PA) = (1 - \phi) \cdot \lambda_{fl}/\lambda_{ex}$. This equation has been successfully used to calculate from photoacoustic data the accepted literature values for the fluorescence quantum yields of many dyes free in solution, such as azulene, 2,5-diphenyloxazole, prodan, acrylodan, and *N*-(5-dimethylaminonaphthalene-1-sulfonyl)glycine, with differences between the literature Φ_{fl} and those calculated from photoacoustic data on the order of ±0.09 or less (Small et al., 1989; Small and Larson, 1990). In comparison, the right-

TABLE 1 Comparison of fluorescence quantum yields (Φ_{fl}) measured by standard fluorescence (fl) methods and by pulsed-laser photoacoustics (PA)

		Fluorescence emission		15°C			25°C			35°C			15–35°C
Sample	PA excitation λ_{ex} (nm)	λ_{max} (nm)	λ_{fl} (nm) for PA calculations	$\Phi_{fl}(fl)$	$\Phi_{fl}(PA)$*	$\Delta\Phi_{fl}$ (PA-fl)	$\Phi_{fl}(fl)$	$\Phi_{fl}(PA)$*	$\Delta\Phi_{fl}$ (PA-fl)	$\Phi_{fl}(fl)$	Φ_{fl} (PA)*	$\Delta\Phi_{fl}$ (PA-fl)	Mean $\Delta\Phi_{fl}$(PA-fl)
ALBP + 1,8-ANS#	366.6	490	490	0.63	0.87	0.24	0.53	0.80	0.27	0.48	0.78	0.30	0.27
ALBP-acrylodan#	366.6	500	500	0.57	0.72	0.15	0.53	0.70	0.17	0.49	0.72	0.23	0.18
ALBP-acrylodan + oleic acid#	366.6	493	493	0.58	0.81	0.23	0.54	0.75	0.22	0.50	0.73	0.23	0.23
IFABP + 1,8-ANS#	366.6	490	490	0.41	0.67	0.26	0.35	0.63	0.28	0.31	0.64	0.33	0.29
IFABP-acrylodan§	366.6	432 (~60%), 510 (~40%)	463	0.38	0.40	0.02	0.33	0.35	0.02	0.29	0.32	0.03	0.02
IFABP-acrylodan + oleic acid§	366.6	510	510	0.33	0.33	0.00	0.33	0.25	−0.08	0.32	0.22	−0.10	−0.06
GFP#	366.6	509 (~80%), 545 (~20%)	515	0.86	1.21	0.35	0.84	1.15	0.31	0.81	1.14	0.33	0.33
GFP#	475.3	509 (~80%), 545 (~20%)	515	0.86¶	1.00	0.14	0.89¶	1.00	0.11	0.94¶	0.98	0.04	0.10
1,8-ANS#	366.6	550	550				0.01	0.02	0.01				0.01
Acrylodan in MeOH	366.6	502	502				low‖	<0.01	0.01				0.01
1,8-ANS in MeOH	366.6	490	490				0.22	0.27	0.05				0.05

* Calculated as $\Phi_{fl} = (1 - \phi) \cdot \lambda_{fl}/\lambda_{ex}$, where ϕ is the photoacoustics single-component amplitude value, λ_{fl} is the fluorescence emission λ_{max} used for PA calculations (the approximate wavelength of median fluorescence energy), and λ_{ex} is the PA excitation wavelength (Small et al., 1989).

$\Phi_{fl}(fl)$ values were obtained with the sample dissolved in 0.1 M Tris-HCl (pH 7.0), whereas $\Phi_{fl}(PA)$ values were obtained with the sample in 10 mM Tris-HCl (pH 7.5).

§ $\Phi_{fl}(fl)$ values were obtained with the sample dissolved in 0.1 M K^+ phosphate (pH 7.0), whereas $\Phi_{fl}(PA)$ values were obtained with the sample in 10 mM Tris-HCl (pH 7.5).

¶ The fluorescence quantum yield reference was fluorescein rather than quinine sulfate.

‖ For ethanol solutions (Prendergast et al., 1983).

hand column of Table 1 shows the mean differences between Φ_{fl}(PA) and Φ_{fl}(fl) over the 15–35°C temperature range. The mean $\Delta\Phi_{fl}$(PA-fl) values are low for the free dyes, 1,8-ANS in buffer, 1,8-ANS in methanol, and acrylodan in methanol, as well as for acrylodan bound to IFABP, in the presence and absence of bound oleic acid. The $\Delta\Phi_{fl}$(PA-fl) values are 0.10 or greater for every other protein system, with the largest differences being 0.27 for 1,8-ANS-labeled ALBP, 0.29 for 1,8-ANS-labeled IFABP, and 0.33 for GFP excited with 366.6-nm light. In calculating fluorescence quantum yields using $\Phi_{fl}(PA) = (1 - \phi) \cdot \lambda_{fl}/\lambda_{ex}$, as done in Table 1, there is a need to determine a single fluorescence wavelength that approximates the wavelength of median fluorescence energy. For molecules with broad, unstructured fluorescence spectra, the emission maximum will suffice for λ_{fl}, incorporating only a very small error (1% or less) into the calculated quantum yield (Small and Larson, 1990). For the GFP and the acrylodan-labeled IFABP samples, however, the emission spectra have two strong features, and an attempt was made to estimate the median of complex emission for quantum yield calculations. In reality, changing the value of λ_{fl} to any fluorescence wavelength in the fluorophore's emission spectrum will change the calculated Φ_{fl}(PA) only slightly.

Fluorescence quantum yields for GFP measured photoacoustically with 366.6 nm photoexcitation were physically unreasonable, having values greater than unity (Table 1). Although 475.3-nm excitation into the visible band of GFP gave calculated Φ_{fl}(PA) values that were physically reasonable, in that they were $\leq$1.0, the fact that they were all higher than the corresponding Φ_{fl}(fl) values forces us to be cautious in their interpretation. The Φ_{fl}(fl) values used to compare the GFP photoacoustic results with 475.3-nm excitation were obtained using fluorescein as a standard.

The crystal structure of GFP has been solved recently (Yang et al., 1996). The fluorophore, which is actually a component of the peptide chain (i.e., is tethered at either end), is buried literally in the middle of a "β-can" structure with no calculable solvent accessibility. Because this moiety has essentially zero fluorescence in almost any solvent medium, its packing into the protein matrix is clearly key to the intense fluorescence. Our results seem to suggest that under such conditions the photoacoustic signal may be anomalously small, implying possible perturbation of that signal because of interactions of the excited fluorophore with the protein matrix.

DISCUSSION

The photoacoustic data we have presented are significant for three major reasons: 1) Most of the fluorophore-protein systems examined exhibited no significant nonthermal, volumetric processes, yet the photoacoustic waveforms resulting from the heat release after photoexcitation were substantially smaller than that expected on the basis of their fluorescence quantum yield determined from standard fluorescence experiments. 2) Only the fluorescent dyes free in solution, and a protein-fluorophore complex in which the covalently bound fluorophore acrylodan may be tethered externally to the protein, showed photoacoustic signals consistent with their measured fluorescence quantum yields. 3) A series of nonthermal volumetric processes were identified for 1,8-ANS bound to a protein, ALBP, which may give insight into the nature of changes induced in the size, shape, and orientation of the fluorophore or its immediate environment upon photoexcitation and subsequent relaxation.

For a metmyoglobin solution at 7°C, with absorbance $A = 0.3$ at the $\lambda = 366.6$-nm excitation wavelength, and $E_o = 10$ μJ pulse energy incident on the sample cuvette, the thermal energy released to solution, E_{th}, is the same as that absorbed, E_{abs}: $E_{th} = E_{abs} = E_o[1-10^{-A}] = 1.2$ μcal. The illuminated volume of our experiment is approximately 11 mm $\times$ 0.5 mm $\times$ 10 mm, or about $V_o = 0.05$ ml. The temperature increase in the illuminated volume as a result of heat deposition is $\Delta T = E_{th}/(C_p\rho V_o) = 2.4 \times 10^{-5}$°C, assuming water parameters $\rho = 1$ g/ml and $C_p = 1$ cal/g-°C. The volume increase ΔV of the solution in response to heat deposition by the photoexcited metmyoglobin is $\Delta V = \beta V_o \Delta T = 5.5 \times 10^{-11}$ ml, where the value for water at 7°C, $\beta = 46 \times 10^{-6}$ (°C)$^{-1}$, is assumed (Weast, 1974). With 366.6-nm excitation, having $E_{h\nu} = 78.0$ kcal/mol, the number of photons that must have been absorbed to account for $E_{abs} = E_{th}$ is $N = E_{abs}/E_{h\nu} = 1.5 \times 10^{-11}$ mol. Finally, the apparent volume change in ml/mol is then ΔV/mol = 4 ml/mol. Thus the volume change giving rise to the metmyoglobin waveforms at 7°C in Figs. 2, 5, and 6 is ~4 ml/mol of photoexcited metmyoglobin molecules.

The nonthermal volume changes represented by the two components in Fig. 6 have uncertain amplitudes due to resolution problems, but may be estimated to be in the range of -2 to -12 ml/mol for the initial contraction, and +2 to

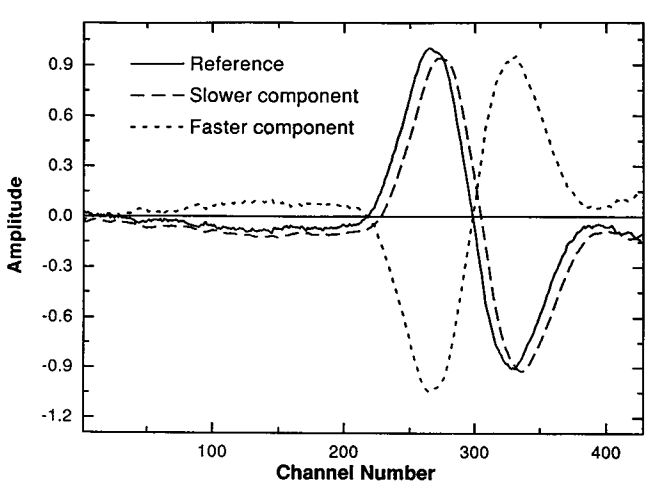

FIGURE 6 The two decay components that sum together to comprise the simulated waveform, which is fit to the sample waveform in Fig. 5. The reference curve is the same metmyoglobin reference waveform shown in Fig. 5, whereas the two decay components are shown individually as the faster component ($\tau < 20$ ns) and the slower component ($\tau \approx 35$ ns).

+12 ml/mol for the subsequent expansion, with the expectation that the absolute values of the contraction and expansion are the same. The value of ±(2–12) ml/mol for a volume change is reasonable, given the magnitude of other volume change measurements that are emerging in the literature on photothermal techniques. For example, volume changes accompanying the bacteriorhodopsin photocycle are on the order of −11, 60, and 145 ml/mol (Schulenberg et al., 1995). Volume changes for the photoinduced electron transfer between xanthene dyes and metal cyanides have been found to be between −5 and +5 ml/mol (Jiwan et al., 1995). The volume changes on the microsecond time range in bacterial photosynthesis involve a contraction of ~7 ml/mol (Malkin et al., 1994). Thus the volume changes estimated here for 1,8-ANS photophysics, in the range of ±(2–12 ml/mol), are similar to other reported photoinduced volume changes in biology and chemistry. Because 1,8-ANS free in solution and bound to IFABP do not show these volume changes, we infer that they are caused by some physical characteristic of the 1,8-ANS–ALBP complex determined by the protein matrix, e.g., solvent reorganization or chromophore changes caused by photoexcitation of the noncovalently resident fluorophore.

Free fluorescent dyes versus those bound inside proteins

Our results show that dyes free in solution or tethered to the surface of a protein (e.g., acrylodan-IFABP), give photoacoustic signals that are reasonably consistent with their known fluorescence quantum yields. In contrast, fluorophores buried "inside" proteins seem to give photoacoustic signals that are substantially smaller than that expected for their known fluorescence quantum yields. Their apparent fluorescence quantum yields from photoacoustic measurements are too high, indicating that their heat-induced waveforms are too small. This was consistent for all of the proteins with what we considered to be buried fluorophores (Table 1).

The explanation for this is not obvious. A large contraction, for example, the negative of the 7°C waveform in Fig. 2, if seen at the $\beta = 0$ temperature and present as well at higher temperatures, could explain a diminished photoacoustic signal, but no such large, long-lived contractions were found. The storage of absorbed photon energy in a long-lived (>10 μs) excited state could also explain the "missing" signal. However, a careful evaluation of a photophysical Jablonski diagram for GFP indicated that a long-lived state (e.g., a triplet) could not explain the signals from GFP for either 366.6-nm or 475.3-nm photoexcitation. In general, the fluorescence quantum yield for GFP is so high to begin with that there is little "opportunity" for the molecule to exhibit alternative decay pathways. Invoking a long-lived, high-energy state as a possibility for GFP would lead to even higher apparent fluorescence quantum yields. The physically unreasonable $\Phi_{fl} > 1.0$ calculated for GFP from photoacoustic data is thus taken to be representative of a systematic feature that is likely to occur for all protein samples with buried fluorophores.

We are thus led to reexamine some of the operating assumptions of the photoacoustic experiment that we have used. The first assumption is that metmyoglobin is a suitable reference compound. Metmyoglobin has been found to be a very good reference compound for aqueous systems, giving acoustic waveforms comparable to those of other suitable reference compounds (Small and Kurian, 1995). Metmyoglobin contains a buried chromophore that absorbs light and releases that absorbed energy rapidly, within 10 ps. The fluorescent proteins with buried chromophores examined in this study are expected to show at least two separate heat deposition processes, the first corresponding to vibrational relaxation from the Franck-Condon state, complete within 2–3 ps, and the second corresponding to the actual decay of the excited singlet, occurring on the time scale of a typical fluorescence lifetime of ~1–10 ns. The main difference, then, between our reference compound and the protein samples with buried fluorescent chromophores is the appearance of a relatively long-lived excited singlet state, with altered physical properties relative to the ground state, and a heat deposition process on the 1- to 10-ns time scale. The instrumentation used in our work integrates all heat deposition processes occurring within the digitization channel width of 10 ns, so in principle, the relatively long-lived singlet states of the fluorescent proteins (1–10 ns) should not be problematic unless they perturb protein structure irreversibly within the experimental resolution of up to 10 μs.

The second assumption is that the thermoelastic parameters used to describe the photoacoustic experiment refer to bulk solvent only and not to the microenvironment of the fluorophore. Usually bulk solvent properties are assumed for calculation purposes. The bulk solvent property most easily measured by the photoacoustic experiment is speed of sound, as indicated in the discussion of Fig. 2. No significant speed-of-sound differences were found between reference waveform and fluorescent protein sample waveforms at the same temperature. Thus the bulk solvent compressibility is likely to be the same for both reference and sample, and other bulk solvent parameters are likely to be the same as well. However, the density, heat capacity, thermal cubic volumetric expansion coefficient, and compressibility of a protein are not likely to be the same as those of the bulk solvent. Furthermore, a protein would be expected to have a hydration shell with properties atypical of those for a bulk solvent. Our anomalous results may be interpreted as arising from photoacoustic signals smaller than expected. If the expected amount of heat were released by the fluorescent proteins, in the absence of significant nonthermal volume changes, then the diminished photoacoustic signals may be due to an apparent β that is lower than expected (i.e., indicative of aqueous solvent properties more like those at a lower temperature), or that the apparent compressibility is

higher than expected (i.e., suggestive of local properties with hydrocarbon nature). The possibility that microenvironment, rather than bulk solvent, determines photoacoustic signals must be further tested for validity.

Two studies to date by other groups have yielded conflicting conclusions on the origin of photoacoustic signals. Both studies were initiated on the premise that water is the worst solvent for photothermal techniques, i.e., aqueous solutions generate smaller photothermal signals than any other solvent. Redmond (Redmond, 1991) used reversed micelles for photoacoustic studies on a water-soluble photosensitizer, Rose Bengal. The approach taken in this study was to achieve the solubilization of the sensitizer in the water core of reversed micelles so that the local environment of the sensitizer was predominantly aqueous but the bulk composition of the solution, being overwhelmingly hydrocarbon, determined the nature of the signals detected. In general, the more hydrocarbon character to the overall solution, the greater the photoacoustic signal detected. In contrast, Tran and Van Fleet (1988) used a related photothermal technique, thermal lensing, to study fluorophores in micelles. In this study, a partial hydrocarbon environment was found to increase both the fluorescence and the thermal signals. (Usually, as fluorescence increases, heat release decreases, because of energy balance considerations.) An enhancement mechanism was proposed in which the fluorescence was enhanced because micelles isolate and protect the fluorophore from quencher molecules as well as increase the viscosity of the medium. The thermal lens enhancement, on the other hand, was suggested to be due to the modification of the thermooptical properties of water by micelles, namely, an increased temperature coefficient of index of refraction, dn/dT, and decreased thermal conductivity. Tran and Van Fleet thus found that fluorophore microenvironment was the key determinant of both luminescent and photothermal signals.

Our study suggests that, through mechanisms not yet understood, the microenvironment of a fluorophore determines the amplitude of photoacoustic signals. In our case, samples were in aqueous solution, and photoacoustic signals were smaller than expected. Thus positioning a chromophore in a protein in water generates signals even smaller than that expected for water, which is understood to be the least photothermally efficient solvent. Further studies mapping out the thermodynamic parameters giving rise to photoacoustic signals will be required to fully understand this phenomenon.

We are grateful for the suggestions and criticisms of Drs. Enoch Small, Louis Libertini, W. Anthony Oertling, Tom Autrey, Bengt Nolting, and Iain Robinson. We are very grateful to William Wessels for taking the fluorescence lifetime measurements. EK thanks Dr. Salah Sedarous for helpful suggestions on data analysis. Radha Nandagopal, Summer Daniels, James Heissenbuttel, Ben Brandli, John Boston, and Meena Nandagopal aided in various aspects of this project.

REFERENCES

Adelhelm, K., W. Faubel, and H. J. Ache. 1990. Laser induced photoacoustic spectroscopy in liquid samples: temperature and solvent effects. *Fresenius J. Anal. Chem.* 338:259–264.

Banaszak, L., N. Winter, Z. Xu, D. A. Bernlohr, S. Cowan, and T. A. Jones. 1994. Lipid-binding proteins: a family of fatty acid and retinoid transport proteins. *Adv. Protein Chem.* 45:89–151.

Blinks, J. R., P. H. Mattingly, B. R. Jewell, M. van Leeuwen, G. C. Harrer, D. G. Allen. 1978. Practical aspects of the use of aequorin as a calcium indicator: assay, preparation, microinjection, and interpretation of signals. *Methods Enzymol.* 57:292–328.

Churio, M. S., K. P. Angermund, and S. E. Braslavsky. 1994. Combination of laser-induced optoacoustic spectroscopy (LIOAS) and semiempirical calculations for the determination of molecular volume changes: the photoisomerization of carbocyanines. *J. Phys. Chem.* 98:1776–1782.

Demas, J., and G. Crosby. 1971. The measurement of photoluminescence quantum yields: a review. *J. Phys. Chem.* 75:991–1024.

Grabowski, J. J., C. R. Bertozzi, J. R. Jacobsen, A. Jain, E. M. Marzluff, and A. Y. Suh. 1992. Fluorescence probes in biochemistry: an examination of the non-fluorescent behavior of dansylamide by photoacoustic calorimetry. *Anal. Biochem.* 207:214–226.

Jiwan, J.-L. H., A. K. Chibisov, and S. E. Braslavsky. 1995. Volume changes associated with electron transfer quenching of excited $Ru(bpy)_3^{2+}$ and xanthene dyes. Time-resolved optoacoustic studies. *J. Phys. Chem.* 99:10246–10250.

Kirk, W. R. 1986. A lanthanide nucleotide complex as a spectroscopic and kinetic probe of phosphoryl transfer. Ph.D. thesis. Johns Hopkins University, Baltimore, MD.

Kirk, W. R., E. Kurian, and F. G. Prendergast. 1996. Characterization of the sources of protein-ligand affinity: 1-sulfonato-8-(1′)anilinonaphthalene binding to intestinal fatty acid binding protein. *Biophys. J.* 70: 69–83.

Kurian, E., F. G. Prendergast, A. J. Tomlinson, M. W. Holmes, and S. Naylor. 1997. Identifying sites of protein modification using MALDI-TOF-MS and on-line membrane preconcentrarion-capillary electrophoresis tandem mass spectrometry (mPC-CE-MS/MS). *J. Am. Soc. Mass Spectrometry.* 8:8–14.

Libertini, L. J. 1996. SOUND 3000 Analysis: Least-Squares Analysis of Photoacoustics Data. Quantum Northwest, Spokane, WA.

Malkin, S., M. S. Churio, S. Shochat, and S. E. Braslavsky. 1994. Photochemical energy storage and volume changes in the microsecond time range in bacterial photosynthesis—a laser induced optoacoustic study. *J. Photochem. Photobiol. Biol.* 23:79–85.

Ockner, R. K. 1990. Historic overview of studies on fatty-acid binding proteins. *Mol. Cell. Biochem.* 98:3–9.

Patel, C. K. N., and A. C. Tam. 1981. Pulsed optoacoustic spectroscopy of condensed matter. *Rev. Mod. Phys.* 53:517–550.

Prasher, D. C., V. K. Eckenrode, W. W. Ward, F. G. Prendergast, and M. J. Cormier. 1992. Primary structure of the *Aequorea victorea* green-fluorescent protein. *Gene.* 111:229–233.

Prendergast, F. G., M. Meyer, G. L. Carlson, S. Iida, and J. D. Potter. 1983. Synthesis, spectral properties, and use of 6-acryloyl-2-dimethylaminonapthalene (acrylodan). *J. Biol. Chem.* 258:7541–7544.

Redmond, R. W. 1991. Enhancement of the sensitivity of radiative and nonradiative detection techniques in the study of photosensitization by water-soluble sensitizers using a reverse micelle system. *Photochem. Photobiol.* 54:547–556.

Richieri, G. V., R. T. Ogata, and A. M. Kleinfeld. 1992. A fluorescently labelled intestinal fatty acid binding protein. Interactions with fatty acids and its use in monitoring free fatty acids. *J. Biol. Chem.* 267: 23495–23501.

Rothberg, L. J., J. D. Simon, M. Bernstein, and K. S. Peters. 1983. Pulsed laser photoacoustic calorimetry of metastable species. *J. Am. Chem. Soc.* 105:3464–3468.

Rudzki, J. E. 1985. The photochemical dynamics and energetics of rhodopsin and myoglobin. Ph.D. thesis. Harvard University, Cambridge, MA.

Schulenberg, P. J., W. Gärtner, and S. E. Braslavsky. 1995. Time-resolved volume changes during the bacteriorhodopsin photocycle: a photothermal beam deflection study. *J. Phys. Chem.* 99:9617–9624.

Slavik, J. 1982. Anilinonaphthalene sulfonate as a probe of membrane composition and function. *Biochim. Biophys. Acta.* 694:1–25.

Small, J. R., J. J. Hutchings, and E. W. Small. 1989. Determination of fluorescent quantum yields using pulsed-laser photoacoustic calorimetry. *In* Fluorescence Detection III. E. R. Menzel, editor. Society of Photo-Optical Instrumentation Engineers, Bellingham, WA. 1054:26–35.

Small, J. R., and E. Kurian. 1995. Volumetric photoacoustic spectroscopy: listening to more than just heat. *Spectroscopy.* 10:27–35.

Small, J. R., and S. L. Larson. 1990. Photoacoustic determination of fluorescent quantum yields of protein probes. *In* Time-Resolved Laser Spectroscopy in Biochemistry II. J. R. Lakowicz, editor. Society of Photo-Optical Instrumentation Engineers, Bellingham, WA. 1204:126–136.

Small, J. R., L. J. Libertini, and E. W. Small. 1992. Analysis of photoacoustic waveforms using the nonlinear least squares method. *Biophys. Chem.* 42:29–48.

Tran, C. D., and T. A. Van Fleet. 1988. Micellar induced simultaneous enhancement of fluorescence and thermal lensing. *Anal. Chem.* 60: 2478–2482.

Ward, W. W. 1979. Energy transfer processes in bioluminescence. *Photochem. Photobiol. Rev.* 4:1–57.

Ward, W. W., C. W. Cody, R. C. Hart, and M. J. Cormier. 1980. Spectrophotometric identity of the energy-transfer chromophores in *Renilla* and *Aequorea* green-fluorescent protein. *Photochem. Photobiol.* 31:611–615.

Weast, R. C., editor. 1974. CRC Handbook of Chemistry and Physics. Chemical and Rubber Company Press, Cleveland, OH. F-5.

Yang, F., L. G. Moss, and G. N. Phillips, Jr. 1996. The molecular structure of GFP. *Nature Biotechnol.* 14:1246–1251.